Int J Adv Manuf Technol (2016) 83:1113–1125
DOI 10.1007/s00170-015-7592-2

ORIGINAL ARTICLE

Factor analysis of machining parameters of fiber-reinforced polymer composites based on finite element simulation with experimental investigation

Chongyang Gao[1] · **Jianzhang Xiao**[1] · **Jiuhua Xu**[2] · **Yinglin Ke**[1]

Received: 31 January 2015 / Accepted: 12 July 2015 / Published online: 6 August 2015

Abstract A three-dimensional (3D) micromechanical finite element (FE) model of machining of fiber-reinforced polymer (FRP) composites was developed in the paper. The FE modeling considers the three phases of a composite, in which the interphase between the fiber and matrix can realize interfacial debonding to represent the failure of composites and allow heat transfer. The machined surface observations and surface roughness measurements of carbon fiber-reinforced polymer (CFRP) composites at different fiber orientations were done firstly, and then, the model predictions of the machining responses, such as cutting force, temperature, and surface roughness, at different fiber orientations were compared with various experimental data for model validation. It is indicated that the three-phase micromechanical model is capable of precisely predicting machining responses and describing the failure modes of fiber shearing or bending related with fiber orientations in the chip formation process. To investigate the complex coupling influences of multiple machining parameters on the key responses of CFRP composites, the single-factor analyses of each machining parameter were first carried out, and then, the multi-factorial analysis of multiple machining parameters was performed based on the orthogonal design of experiment and the analysis of variance (ANOVA) to quantitatively compare the influences of these key machining parameters on the cutting force and surface roughness. It was found that the fiber orientation angle, depth of cut, and cutting speed prove to be the important factors affecting the cutting force and surface roughness and that the coupling effects of these machining parameters all are relatively negligible in the machining of CFRP composites.

Keywords Factor analysis · Machining parameters · Fiber-reinforced polymer (FRP) composite · Micromechanical finite element (FE) modeling · Surface measurement

1 Introduction

Fiber-reinforced polymer (FRP) composites with high strength, light weight, and fatigue and corrosion resistances consist of various polymer matrices and long fibers. Owing to their excellent mechanical properties, FRP composites are becoming the promising solutions to various industrial applications [1, 2] especially used as structural components in the weight-critical aerospace industry. Despite the fact that composite parts are fabricated near-net shape, machining operations such as trimming and drilling are still required in order to achieve close fit tolerances and finalize part sizes. The machining of the FRP composites differs significantly from that of traditional metal materials. The cutting process of mostly homogeneous materials is characterized by plastic deformation of the bulk material with continuous chip, while the cutting mechanism of FRP composites is characterized by the anisotropy and non-homogeneity nature. For the structure of the FRP composites, the matrix phase and interfacial phase are the constituents that provide load transfer and structural integrity, while the reinforcement phase enhances the mechanical properties of FRP composites. Considering that the distinct constituents of composites with drastically different mechanical and thermal properties cause the complexity of FRP

✉ Jiuhua Xu
jhxu@nuaa.edu.cn

[1] The State Key Laboratory of Fluid Power Transmission and Control, College of Mechanical Engineering, Zhejiang University, Hangzhou 310027, China

[2] College of Mechanical and Electrical Engineering, Nanjing University of Aeronautics & Astronautics, Nanjing 210000, China

composites, extensive studies on machining mechanisms of FRP composites have been carried out as introduced below.

The integrity of the machined surface is a fundamental aspect in determining the machinability of FRP composites. And, the structural quality can be significantly affected by the machined surface where some defects such as delamination, cracking, fiber pullout, and burning can occur [3–5]. Therefore, extensive experimental tests have been performed with the intention of investigating the quality of the cutting surface for different cutting conditions in the FRP composites machining. An end-milling test on carbon nanotube reinforced composites has been conducted in [6], in which the surface roughness under various cutting parameters has been investigated by using the analysis of variance. The multiple regression analysis model of the surface roughness was offered to reveal the significant effects of feed rate, spindle speed, and depth of cut on surface quality in milling [7] and turning [8] glass FRP composites. A mathematical model of surface roughness was further studied based on the response surface methodology [9, 10]. The circumferential milling process of unidirectional carbon fiber-reinforced polymer (CFRP) composite was performed to investigate the effect of milling parameters such as cutting speed, fiber orientation, and workpiece temperature on the surface integrity [11].

On the other hand, the cutting force is the other fundamental aspect in determining the machinability of FRP composites, which is also strongly influenced by the machining parameters and the properties of workpiece and tool. Some experimental works of various manufacturing process (e.g., milling, drilling, trimming, etc.) have been done to investigate the cutting force [12, 13], while numerical simulation works were performed to analyze the cutting force by using the micromechanical and macroscopic finite element method [14–16]. Furthermore, some analytical models were also proposed to predict the cutting force in FRP composites [17–19].

Due to the anisotropic and inhomogeneous properties of FRP composites, the interaction between the FRP composites and the tool is very distinguishably different from that of homogeneous materials. The investigations of chip formation and material removal mechanisms in FRP composites machining can provide the essential knowledge to understand the interaction between FRP composites and tool. To get a better understanding of the chip formation process and damage initiation and propagation, a 2D numerical progressive failure analysis was developed by Lasri et al. [20] to investigate the effects of fiber orientation and failure criteria on CFRP laminates. The failure mechanisms at different fiber orientation angles in cutting a CFRP composite were revealed by a micromechanical finite element model with experimental validation [21]. Based on the samples with four different fiber orientations, the chip shapes and rupture modes were analyzed through the orthogonal cutting of carbon/epoxy laminae [22]. More recently, a three-dimensional (3D) finite element model of CFRP orthogonal cutting with cohesive interactions was established to accurately predict material removal phenomenon [23]. Besides, the discrete element method can also be used to describe the chip formation mechanism [24].

Despite the efforts as mentioned above have been devoted to investigate key machining responses of FRP composites (such as the cutting force, machined surface roughness and chip morphologies) by both experimental tests and finite element (FE) simulations, there still exists a challenge to make a quantitative comparative analysis of the coupling influences of multiple machining parameters on certain responses, so as to get an optimal design of the machining process of FRP composites. The present work is devoted to develop a 3D micromechanical FE model with consideration of the three phases (i.e., fiber, matrix, and the interphase between the fiber and matrix) of FRP composites. The effects of each machining parameter on the machining responses will be analyzed firstly by using FE simulations. Based on the simulation results, the multi-factorial analysis is used to study the coupling influences of multiple machining parameters on the machining responses of CFRP composites, so as to determine the most important machining parameters and give a quantitative comparison of their influences. At the same time, the observations and roughness measurements of the machined surfaces at different fiber orientations were also done in this paper for the validation of the FE model.

2 Experiment setup of milling carbon fiber-reinforced polymer composites

The CFRP composites used in our tests were fabricated from the IMS/X850 prepregs with T800 carbon fiber. Four types of laminae were selected in the experiments, in which the fiber orientations are 0°, 45°, 90°, and 135°, respectively. The fiber volume fraction for these laminae is 65 %. The mechanical properties of IMS/X850 prepreg as well as its constituents are given in Table 1. The CFRP laminae with 32 plies have a thickness of 6 mm and were cut into 200×150 mm using diamond-edged saw to fit the clamp.

All the milling experiments were carried out on a DMG Ultrasonic 20 Linear high-speed machining center at the Nanjing University of Aeronautics & Astronautics, as illustrated in Fig. 1. This equipment has maximum spindle speed of 42, 000 rpm and maximum feed speed of 5 m/min. The machining process was performed with a diamond-coated and cemented carbide end mill tool of 10-mm diameter. The machining conditions employed for each test were as follows: cutting speed is 157 m/min, feed rate is 1000 mm/min, axial depth of cut is 6 mm, and radial depth of cut is 1 mm.

To evaluate the machined surface quality of the workpiece samples after milling experiment, the machined surfaces were observed by a Hitachi S-3400N scanning electron microscope

Table 1 Mechanical properties of the IMS/X850 prepreg

Constituent	Properties	Values
IMS/X850 prepreg	Elastic constants	E_{11}=195*GPa*, E_{22}=8.6*GPa*, G_{12}=4.57*GPa*, υ_{12}=0.33
	Tensile strength	X_T=5.49 GPa
	Diameter	d_f=10 μm
Carbon fiber	Elastic constants	E_{f11}=294 GPa, E_{f22}=15 GPa, G_{f12}=15 GPa, υ_{f12}=0.3
	Tensile strength	X_T=2.678 GPa
Epoxy	Elastic constants	E_m=3.1 GPa, υ_m=0.35
	Tensile strength	X_T=70 MPa
	Shear strength	S_m=70 MPa

(SEM). And, then the machined surface roughness of the composite workpiece was measured by MAHR-Perthometer M1 instrument, as shown in Fig. 2. Each measurement was repeated three times, and their average values were taken as the effective ones.

3 FE modeling of fiber-reinforced polymer composites

3.1 Description of three-dimensional cutting finite element model

Considering the microstructure of three individual phases (i.e., fiber, matrix, and the interphase between the fiber and matrix) of the FRP composites, a 3-D micromechanical FE cutting model was established for FRP composites, as shown in Fig. 3. The orthogonal cutting simulation was carried out by using the explicit module of the general FE software ABAQUS/Explicit. The tool was assumed to be a rigid body. The nose radius of the tool is 5 μm, and the rake and relief angles are 25° and 10°, respectively. The tool was given a

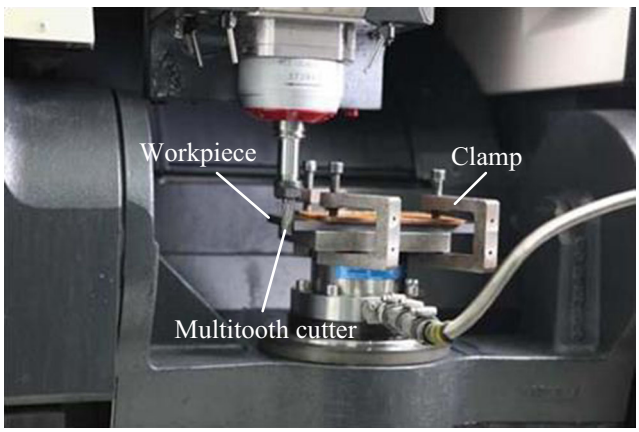

Fig. 1 Experimental setup of milling CFRP composites

Fig. 2 MAHR-Perthometer M1 instrument for the measurement of machined surface roughness

constant cutting velocity in the x direction during the cutting process, the movement of which in the y direction was constrained in the model. The size of workpiece was adopted as 215×215×50 μm (L×H×W). The workpiece was meshed with eight-node brick elements with reduced integration (C3D8R), and there are about 100,000 elements with a minimum element length of 0.5 μm along the cutting path. The initial temperature of the workpiece is set as 25 °C. The displacements were constrained in three directions (x, y, and z) at the bottom surface of the workpiece, and the longitudinal displacement (U_x) was restricted at the left-hand surface of the workpiece. The fiber in the composite workpiece has a hexagonal array arrangement as illustrated in the figure. The fiber orientation angle was defined relative to the cutting path in a clockwise direction. The thickness of interphase was evaluated as 0.5 μm based on the fiber diameter. A kinematical

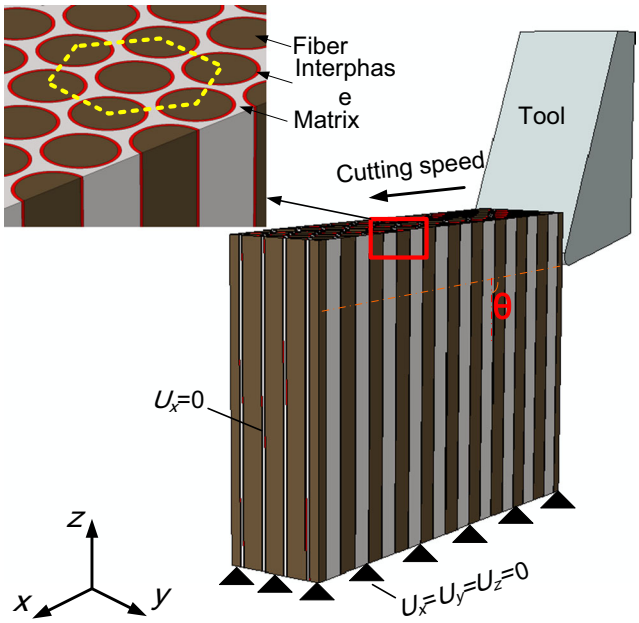

Fig. 3 Illustration of 3D micromechanical FE model of orthogonal cutting of FRP composites (fiber orientation angel θ=90°)

contact definition was applied between the tool surface and workpiece based on the penalty function principle, and the heat partition between the tool and chip was defined as 20 to 80 %. A self-contact condition was adopted for each phase of the composites to avoid penetration among deleted elements during cutting process.

Considering that there exists a large amount of heat transmitted from the tool to the workpiece, the heat conduction between the tool and workpiece was introduced in the FE model so as to consider the thermal phenomenon in machining CFRP composite. The thermal properties of the three phases provided by [25, 26] are given in Table 2. Due to the elastic brittle behavior of CFRP, the heat generated by plastic deformation is negligible and the unique heat source taken into account in the model was produced by the friction at the contact surface between the tool and workpiece. The friction between the cutting tool and fiber plays an important role in the machining of composites. The Coulomb friction law is applied to various contact surfaces. According to the orthogonal machining tests [27], the coefficient of friction between the tool and fiber used in the present micromechanical model was taken as 0.3, 1.8, 0.49, and 0.6 for the 0°, 45°, 90°, and 135° fiber orientations, respectively.

3.2 Material modeling

Contrary to the equivalent homogenous material (EHM) method used in FE machining models, the 3D micromechanical cutting model was built with consideration of the three constituents of the FRP composites. As a real region observed in experiment [28], the interphase was modeled by using a solid continuum element and has been used to realize the failure of materials by interfacial debonding. The cohesive zone model (CZM) is often employed to model the interface between the fiber and matrix; however, it is not suitable for an explicit dynamic simulation because the CZM not only dramatically increases the computational time but also induces excessive element distortion for compressive failure. Therefore, the constitutive models and damage models for the three constituents of the FRP composites are required.

Table 2 Thermal properties of the three phases in the adopted CFRP composite

Constituents	Properties	Values
Carbon fiber	Longitudinal thermal conductivity, λ_L (W/m K)	9.37
	Transverse thermal conductivity, λ_T (W/m K)	4
	Longitudinal thermal expansion, α_L (10^{-6}/K)	−0.41
	Transverse thermal expansion, α_T (10^{-6}/K)	10.5
	Specific heat, C_p (J/kg/K)	794
	Thermal conductivity, λ_c (W/m K)	0.22
Epoxy	Thermal expansion, α_L (10^{-6}/K)	72
	Specific heat, C_p (J/kg/K)	1210
	Thermal conductivity, λ_c (W/m K)	2.52
Interphase	Thermal expansion, α_L (10^{-6}/K)	27.6
	Specific heat, C_p (J/kg/K)	990.8

1. Fiber and matrix models

The carbon fiber is assumed to be an elastic and anisotropic material and can be fully characterized by the anisotropic elasticity moduli of the fiber (E_f). It has been observed that the carbon fiber has small fracture toughness and has not significant plasticity before failure. Therefore, the carbon fiber is assumed to fail at the onset of the stress of the fiber exceeding the anisotropic ultimate strength. The epoxy matrix of the composite is modeled as an isotropic and elasto-plastic material, the elastic behavior of which is characterized by the elastic modulus (E_m) and the Poisson ratio (υ_m), and the plastic behavior is described by von Mises yield criterion and isotopic hardening. It can be assumed for the epoxy matrix that the yield behavior is independent of the hydrostatic stress and the yield behavior is equal in tension and compression. The damage begins when the stress in the matrix reaches the yield strength. The elastic modulus of matrix linearly degrades with microcracks generated in the matrix and becomes zero at an equivalent plastic strain of 0.05 corresponding to final fracture.

2. Interphase model with damage failure

The solid continuum element has been used to represent the interphase between the fiber and the matrix which is better than the CZM in the cutting simulation. The interphase is defined as an isotropic elastic material (the elastic modulus is denoted by E_i). A progressive damage happens at the maximum normal and tangential stress (σ_{max} and τ_{max}). The normal damage behavior of the interfacial elements is modeled with a tensile progressive damage model, which describes the normal separation of the interface. After damage initiation occurs, the degree of damage can be fully characterized by a scalar damage variable (D). As the normal strain increases, the current state of damage exhibits itself in the form of a decrease modulus of elasticity (E_i^d) as shown below:

$$E_i^d = (1-D)E_i \tag{1}$$

where E_i^d is the damaged elastic modulus of interphase. The material stiffness is equal to zero when the damage variable is equal to unity which means that the material fully reaches fracture. The damage variable is then said to linearly evolve according to the following:

$$D = \frac{L_e}{u_f^{pl}} \varepsilon^{pl} \tag{2}$$

where L_e is the characteristic element length, ε^{pl} is the plastic strain, and u_f^{pl} is the equivalent plastic displacement at failure which is expressed as

$$u_f^{pl} = \frac{2G_f}{\sigma_y} \tag{3}$$

where G_f is the fracture energy of the material, and σ_y is the static yield stress before the initiation of damage. The equivalent plastic displacement at failure can be determined when G_f is known which is defined as

$$G_f = \sqrt{G_n^2 + G_t^2} \tag{4}$$

and

$$\begin{aligned} G_n &= \int_0^{\varepsilon_f} \sigma d\varepsilon \\ G_t &= \int_{-\gamma_f}^{\gamma_f} \tau d\gamma \end{aligned} \tag{5}$$

where G_n and G_t are the normal and tangential fracture energies, respectively; ε_f is the normal failure strain, and γ_f is the shear failure strain. Besides, the strain at the beginning of damage evolution was also empirically evaluated in the calculation of G_f. Similarly, the shear damage of the interfacial elements is also modeled with the progressive damage approach to account for the failure of FRP composites under shear strains.

4 Simulation results and experimental validation

In the present work, a simulation investigation was carried out to comprehensively study the key machining responses with variation of machining parameters for different fiber orientation angles in CFRP composites. The influences of machining parameters of CFRP composites were analyzed mainly for cutting force, temperature, and surface roughness at respectively corresponding machining conditions.

4.1 Cutting force and temperature and validation

The cutting force is a most important factor in investigating the machinability of CFRP composites. It is produced due to the sliding of the cutting tool against the workpiece to remove the material from the workpiece. The main factors affecting cutting force include machining conditions (such as cutting speed, feed rate, and depth of cut) and the properties of the workpiece and tool. So, the cutting force of a CFRP composite will depend on the machining conditions providing that the cutting tool and workpiece are given. It is worth noting that when the FE predictions of cutting forces were compared with experimental data for validation, all the parameters used in FE model are the same as those in the corresponding experiments. Especially, the thermal properties of the three phases in the FE model were adopted for temperature validation, as shown in Table 2.

The orthogonal micro-machining experiments of CFRPs were performed by Calzada et al. [21] on a three-axis CNC micro-scale machining testbed, in which Kistler 9018 and high-speed camera were used to monitor the cutting process. The cutting speed is 0.5 m/min, and the depth of cut is 30 μm. The relation of the principal cutting force along the cutting direction versus time obtained in FE simulation was presented and validated by the experimental average value of cutting force [21], as shown in Fig. 4a. And, the historical variation

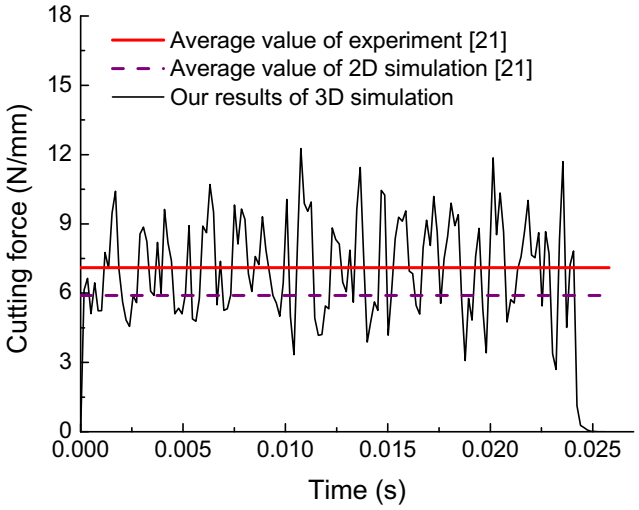

(a)

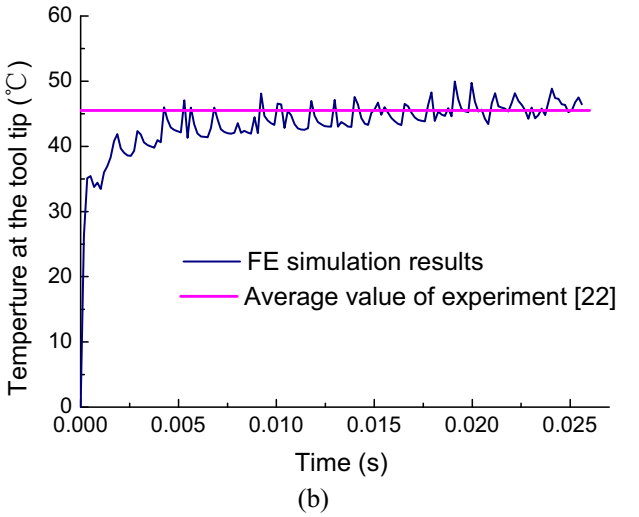

(b)

Fig. 4 The comparisons of the simulated results and the average values of experiments of **a** cutting force and **b** cutting temperature for CFRPs at a fiber orientation of 90°

of the temperature at the tool tip was given and compared with experimental data by Zitoune et al. [22], as shown in Fig. 4b. It can be seen that the simulation results of the cutting force and temperature were in good agreement with the experimental data. Especially, the cutting force predicted by the 3D FE model was closer to the experimental data than the 2D FE model. The temperature shows an unimportant role in the machining of CFRP composites due to its very limited varying range (25 to 46 °C) during the machining process.

As shown in Fig. 5, there is a very good agreement between the predicted and measured [21] values of the average cutting force at different fiber orientation angles in the machining of CFRP composite. It can be seen that the cutting force depends on the fiber orientation and that the cutting force is minimum at 45° and maximum at 90°. This is because shearing of the fiber and matrix is the dominant damage at 45°, and the fibers are simultaneously bent and sheared in bulk at 90°, while the shear failure stress of fiber (380 MPa) is much lower than that in bending (1600 MPa). Although the thrust force was significantly underestimated due to elements that were deleted in the simulation, the simulated results of the thrust force varying with fiber orientations also agree with the experimental data [21].

4.2 Surface roughness and experimental validation

Surface roughness plays a predominant role in determining the machining accuracy. It is noted that the surface roughness of CFRP composites depends on many factors, such as fiber orientation, cutting speed, feed rate, and depth of cut, for a given machine tool and workpiece setup. In reality, the machined surface of CFRP composites differs from that of conventional metallic materials in many respects. Because the cutting surface of CFRP composite is resulted from material removal with the combination of bending, crushing. and shearing and depends on the surface texture of the workpiece, which is closely related with fiber orientation, fiber arrangement, interfacial bonding strength, and the thermomechanical properties of fiber and matrix.

The average surface roughness (R_a), the arithmetic mean of the departures of roughness profile [29], is adopted in this study as follows:

$$R_a = \frac{1}{MN}\sum_{j=1}^{N}\sum_{i=1}^{M}\left|H\left(x_i, y_j\right)\right| \tag{6}$$

where $H(x_i,y_j)$ is the deviation of the profile and M and N are the sampling points which are chosen along the cutting path and perpendicular to the cutting direction, respectively.

The comparisons of the simulated and experimental results of surface roughness of T800/Epoxy at different fiber orientations are presented in Fig. 6, in which the material and cutting conditions adopted in FE simulation are the same as those used in our tests, as shown in Table 1. It is indicated from the figure that the simulation predictions match well with the measured values of average surface roughness at different fiber orientation angles. And, the machined surface is relatively smooth at the orientation angle of 45° while more uneven at 135° (or −45°).

Meanwhile, we have observed the surface topographies of the studied composite at four fiber orientation angles by using Hitachi S-3400N SEM, as shown in Fig. 7. It was shown that the machined surface is mainly composed of bare fibers and resin ridges at 0°. The machined surface is relatively smooth at the 45° fiber orientation, and the poor surface occurs at 135° in

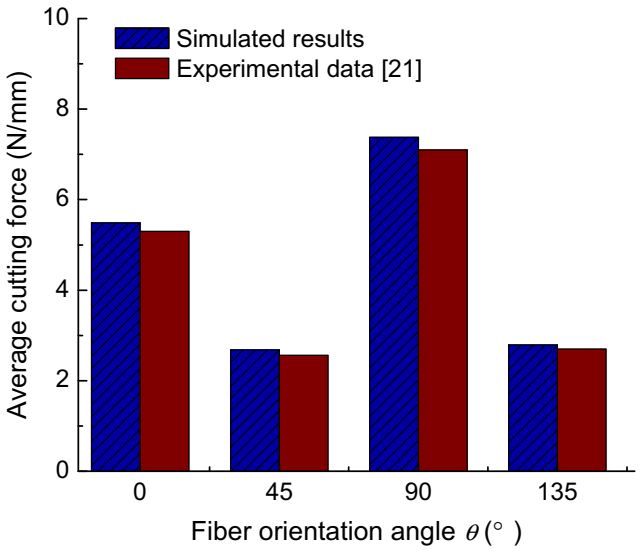

Fig. 5 Experimental validation of the average cutting forces at different fiber orientations

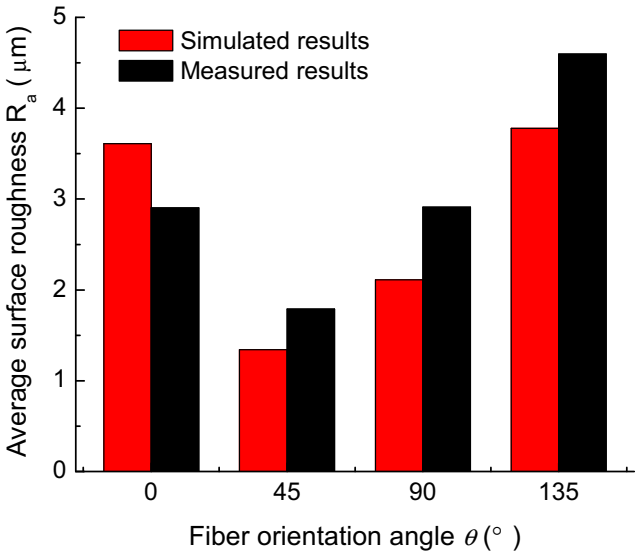

Fig. 6 Comparison of average surface roughness between simulation and our measurement for T800/Epoxy at different fiber orientations

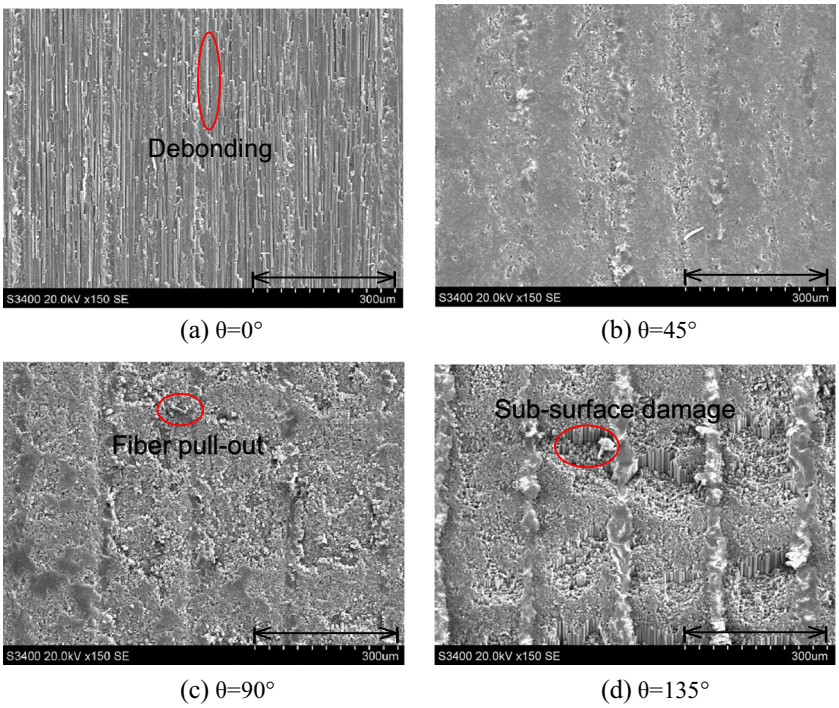

Fig. 7 Observations of the surface topography of T800/Epoxy at **a** 0°, **b** 45°, **c** 90°, and **d** 135°

the CFRP composite. The big pits of carbon fiber bundles and resin ridges were obviously observed at 135° while some small pits on the coated resin layer were found at 90°. Furthermore, the local machining damages such as fiber-matrix debonding at 0°, fiber pullout at 90°, and subsurface damage at 135° have been found in these micrographs (as marked by red circles in the figure).

The simulated results of surface profile of T800/Epoxy at four fiber orientation angles are shown in Fig. 8. It can be seen that the roughness profiles are of fluctuation type for all cases

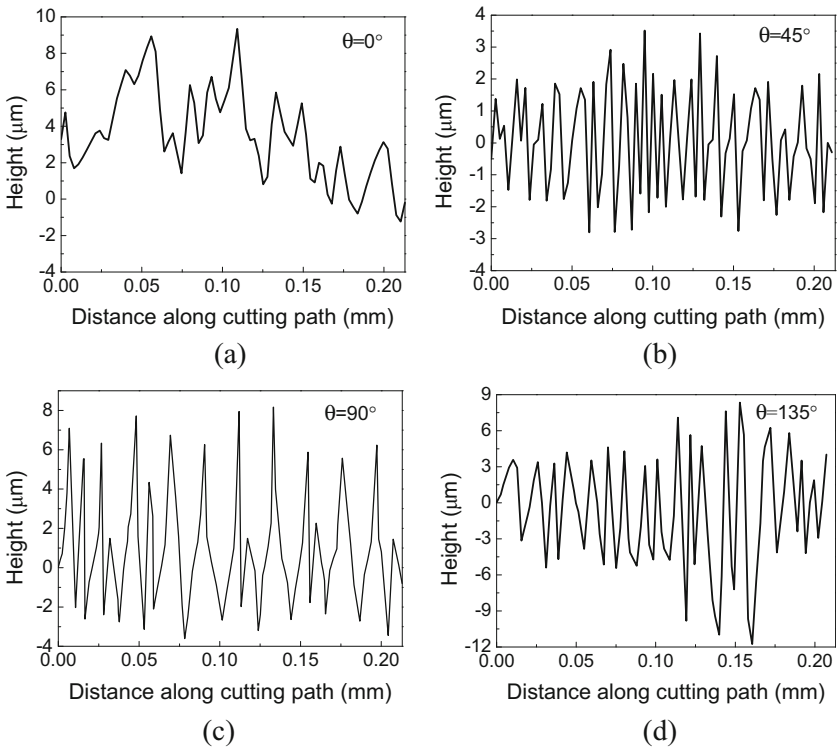

Fig. 8 The simulated results of surface profile of T800/Epoxy at **a** 0°, **b** 45°, **c** 90°, and **d** 135°

of different fiber orientations. The fluctuating magnitude at 45° is obviously lower than those in other cases. The roughness profile at 135° is not as regular as the other three ones, and its valleys are the deepest. These profiles confirm that surface roughness greatly depends on fiber orientation. Especially, the characteristics of these profiles predicted in FE simulation show a very good agreement with those observed in the experiment as presented in Fig. 7.

4.3 Chip morphologies with different failure modes

Since the machining quality obviously decreases at the end of tool life for higher degrees of damage induced on the surface of workpiece, the study on chip formation during machining operation has served a pivotal role on fundamental insights into the optimization of tool life and machining quality. To get better tool life and machining quality for CFRP composites, the numerical simulations of chip formation were done here to reveal the mechanism of material removal of CFRP composites.

Table 3 The different levels of key machining parameters used in factor analysis

Machining parameters	Levels
Fiber orientation angle (θ) (°)	45, 90, 135
Cutting speed (V_c) (m/min)	60, 300, 600
Depth of cut (a_p) (μm)	30, 50, 70

The chip morphologies and various failure modes at different fiber orientations in the machining simulations are shown in Fig. 9. It was indicated in Fig. 9a that the fiber and the matrix separate due to interphase debonding failure when the tool enters the workpiece at 0°. The separation is propagated with the advance of the tool because of bending and compression onto the fiber and matrix. The separation ceases to propagate, and the break happens when the fiber reaches a critical length. The chip is formed when the bending stress exceeds the failure stress of fiber in a direction perpendicular to the fiber orientation, which is reproduced in a cyclic way

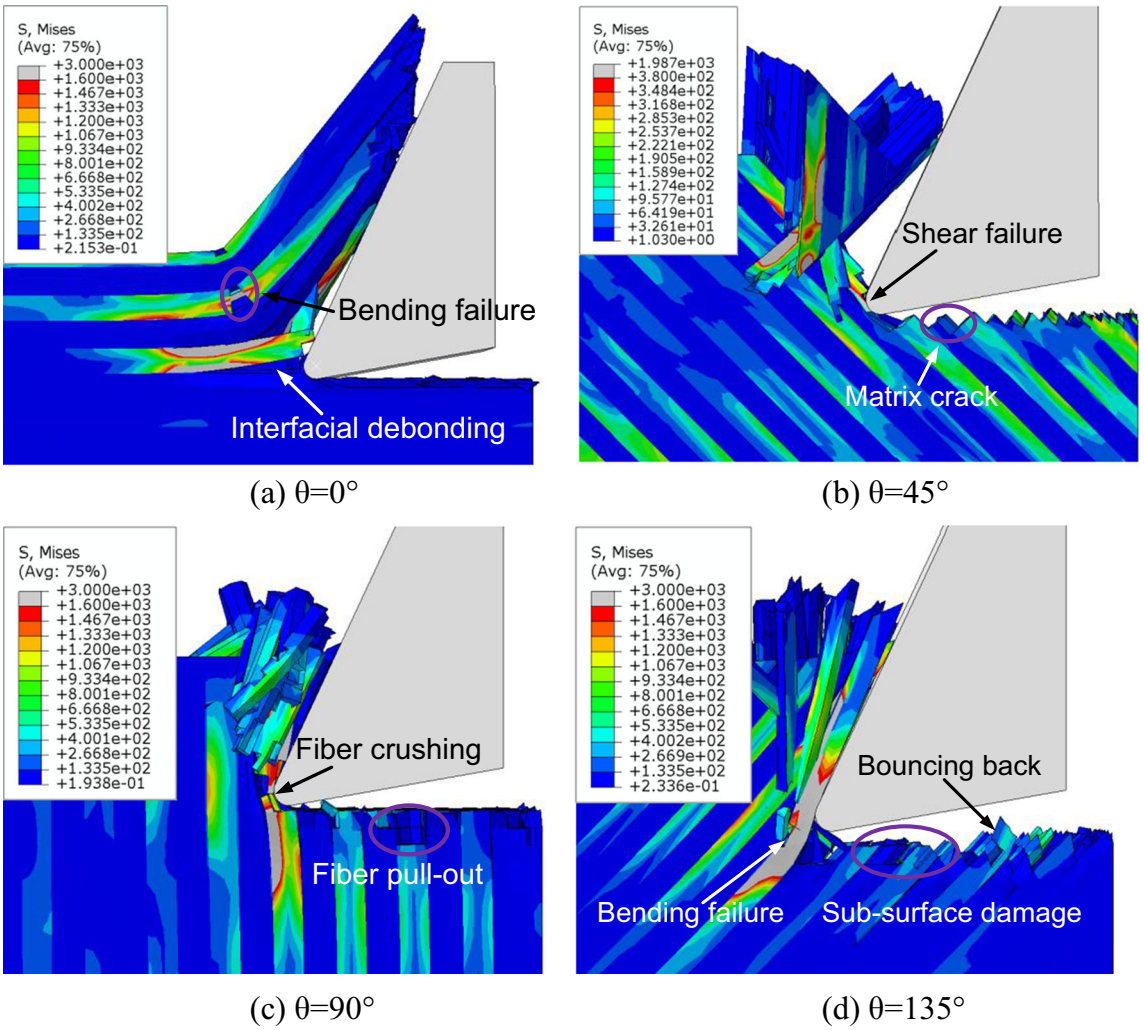

Fig. 9 The chip morphologies and failure modes at different fiber orientation angles

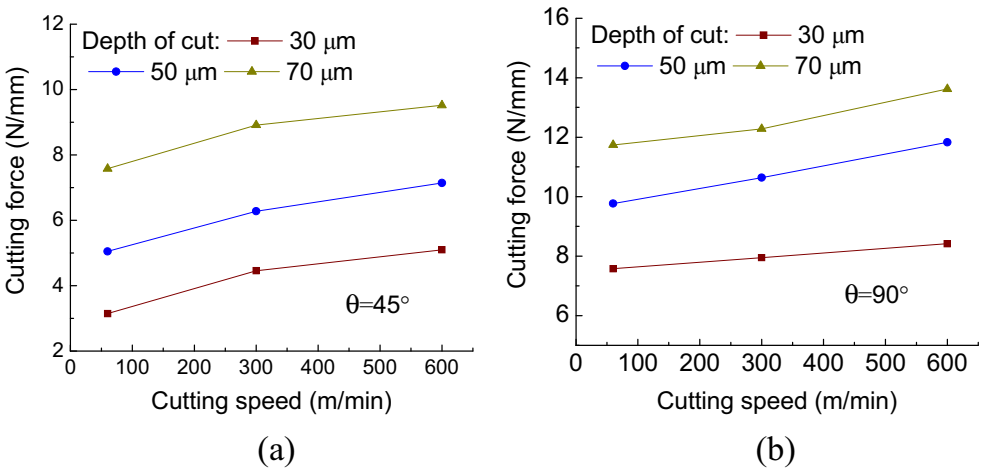

Fig. 10 Dependence of cutting force on the cutting speed at **a** 45° and **b** 90°

until the end of machining. For the case at 45° as shown in Fig. 9b, the fibers and matrix are purely sheared by the compression of the tool. It was found that a shear fracture occurs along the interface during the cutting process. Consequently, the chips are formed with the continuous fiber ruptures caused by shearing and are detached collinearly along fiber orientation resulting in relatively small surface damage.

For the case at 90° as shown in Fig. 9c, the workpiece material is initially loaded by bending ahead of the tool on the fiber-matrix interface and then followed by shearing. The interphase continues to fail as the bending stress in each fiber exceeds its failure value. A discontinuous chip is then generated. Bending stress also occurs below the cutting plane without leading to subsurface fiber failure during the cutting process, but it can result in subsurface damage such as fiber pull-out and delamination at the end of cutting on the machined surface. For the case at 135° as shown in Fig. 9d, the shear failure of matrix and interphase first occurs. Then, the bending fracture in fibers occurs around the cutting surface due to the compression forces of the tool. A discontinuous long chip is formed finally when the compressive stress localized in the cutting edge generates the crack in the interface. In simulation, a bouncing back of fiber was observed, which causes brushing between the relief surface of tool and the machined surface and contributes to the cutting force.

5 Factorial analysis of machining parameters

It is well known that the machined quality of FRP composites is affected by many factors during the machining process. To provide a better understanding of the optimized machining quality, the significance of multiple machining parameters was studied based on the statistical method. By using the analysis of variance (ANOVA), the dominant machining parameters and coupling of double parameters affecting the cutting force and surface roughness were determined by quantitative comparison.

5.1 Analysis of variance

Analysis of variance (ANOVA) is a robust statistical method to obtain some important process parameters which significantly affect the machining responses. This is accomplished by separating the total variability of the multi-performance characteristic index, which is measured by the sum of the

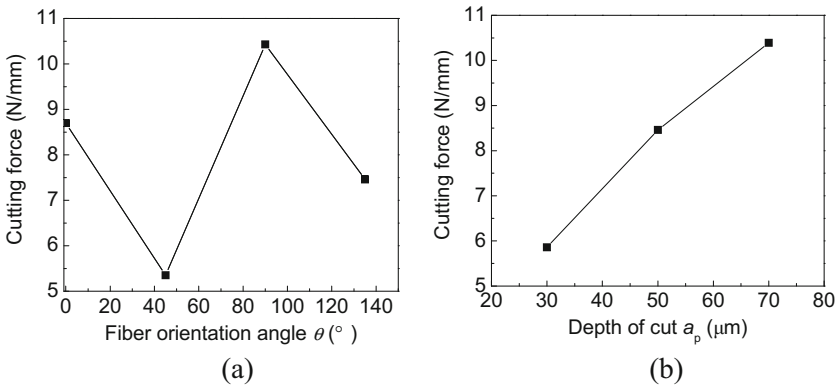

Fig. 11 Dependence of cutting force on **a** fiber orientation angle and **b** depth of cut

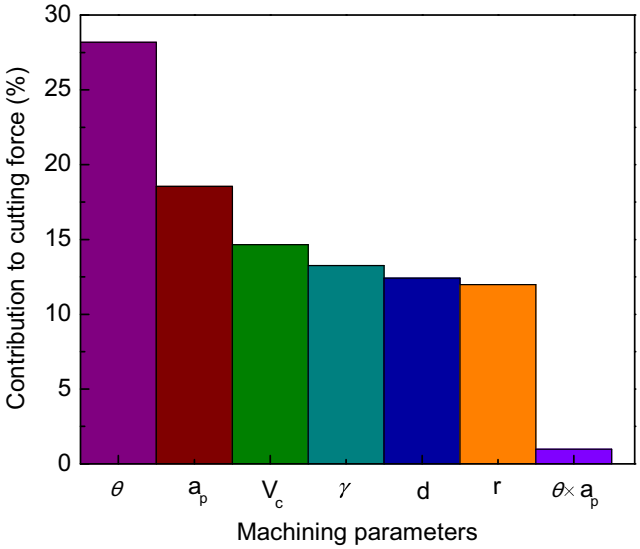

Fig. 12 Quantitative comparison of the contributions of different machining parameters to the cutting force

squared deviation from the total mean of square, into contribution by each of the process parameter. In addition, the F test is used to determine which process parameter has a significant effect on a characteristic performance. So, the F value generally represents the important degree of the process parameter on the performance characteristic.

When applying ANOVA, there are three key assumptions that should be satisfied as follows: (1) the observations are obtained independently and randomly from the populations defined by the factor levels, (2) the population at each factor level is approximately normally distributed, and (3) these normal populations have a common variance, σ^2. That is to say, for factor level i, the population is assumed to have a distribution which is $N(\mu_i,\sigma^2)$. To perform the ANOVA, the principal computational formulae needed are given below

$$\mathrm{SS_T} = \sum_i \sum_j x_{ij}^2 - \frac{T^2}{n} \tag{7}$$

$$\mathrm{SS_B} = \sum_i \frac{T_i^2}{n_i} - \frac{T^2}{n} \tag{8}$$

$$\mathrm{MS_B} = \frac{\mathrm{SS_B}}{N-1} \tag{9}$$

where $\mathrm{SS_T}$ is the total sum of square, $\mathrm{SS_B}$ is the sum of square at all levels for a single factor, and $\mathrm{MS_B}$ is the mean value of $\mathrm{SS_B}$. x_{ij} is the jth observation in the ith level, T is the sum of all n observation values, and n is the total number of observations; T_i is the sum of n_i observation values in the jth level, n_i is the number of observations in the ith level, and N is the number of levels. In this paper, ANOVA was performed by using the software of Statistical Product and Service Solutions (SPSS). The SPSS has been widely used for statistical analysis in various research fields, which include bi-variable statistics, descriptive statistics, and multi-variable ANOVA. Especially, ANOVA has become an important module of the statistical analysis tool.

5.2 Results of analysis of variance

In this paper, a series of simulations were performed to provide the sample data needed in ANOVA, so as to investigate the effects of machining parameters and coupling of double parameters on the cutting force and surface roughness. The different levels of key machining parameters used in factor analysis are listed in Table 3 based on design of experiment.

The single-factor analyses of the effects of three key machining parameters on the cutting force were firstly carried out, as presented in Figs. 10 and 11. The effect of the cutting force is studied in Fig. 10 for two typical fiber orientation angles of 45° and 90°. It can be seen that the cutting force increases with the increase of cutting speed at both cases, and the increasing trend also exists for all the fiber orientations. Furthermore, although the increase of cutting speed can lead to high cutting temperature in the shear zone and hence softens the workpiece [30], the cutting force did not drop in

Table 4 Results of the analysis of variance for cutting force

Machining parameters	Sum of squares ($\mathrm{SS_B}$)	Degrees of freedom	Mean square ($\mathrm{MS_B}$)	F value	p value
Fiber orientation angle (θ)	72.3	3	24.1	5.72	0.000
Depth of cut (a_p)	31.72	2	15.86	3.07	0.000
Cutting speed (V_c)	25.04	2	12.52	1.959	0.000
Rake angle (γ)	11.34	1	11.34	1.823	0.000
Fiber diameter (d)	10.62	1	10.62	1.745	0.000
Edge radius (r)	10.24	1	10.24	1.675	0.000
Interaction ($\theta \times a_p$)	5.04	6	0.84	0.134	0.001

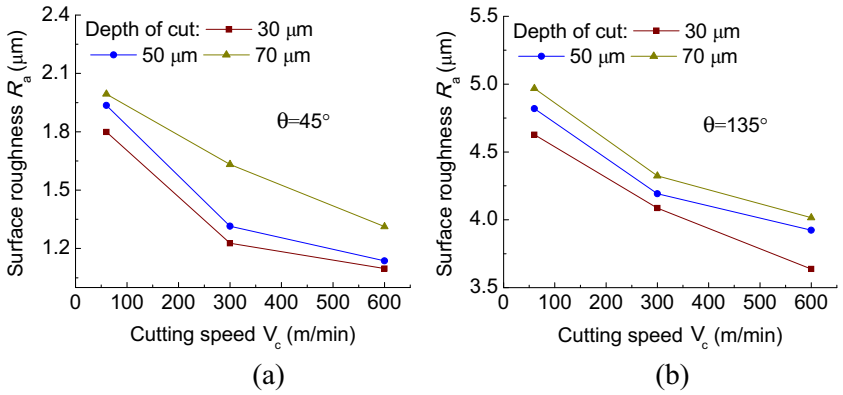

Fig. 13 Dependence of surface roughness on cutting speed at **a** 45° and **b** 135°

our simulation mainly because the elevated magnitude of cutting temperature is very small during the machining process. In Fig. 11a, b, the relations of cutting force versus the fiber orientation angle and depth of cut were plotted, respectively. It can be known from the figures that the results of the maximum cutting force are observed at 90° while the lowest cutting force at 45°, as shown in Fig. 11a, and the cutting force is almost linearly increasing with the depth of cut in Fig. 11b.

As shown in Fig. 12, the multi-factorial analysis based on the orthogonal design of experiment was further used to study the effects of multiple machining parameters and their coupling effects on the cutting force. The results of multi-factorial ANOVA for cutting force are listed in Table 4. These analyses were carried out for a level of significance of 5 %; i.e., the default p value is 0.05. It was found that fiber orientation angle (θ), depth of cut (a_p), and cutting speed (V_c) have the most significant levels for the cutting force and that the coupling effects of two factors (such as fiber orientation and depth of cut) are actually quite small and can be neglected in the analysis.

At the same time, the single-factor analyses of the effects of three key machining parameters on surface roughness were also carried out, as presented in Figs. 13 and 14. The dependence of the surface roughness of the cutting speed was plotted for the two orientations of 45° and 135° in Fig. 13. It can be clearly seen in the figure that the surface roughness gradually decreases with increasing cutting speed, which indicates that the higher cutting speed is good for machined surface of CFRPs. In addition, a slight increase in surface roughness was observed when the depth of cut increases from 30 to 70 μm, which implies that larger depth of cut is not preferred for higher surface quality in machining CFRP composite. These simulated results are in good agreement with the experimental data [7, 8]. The relations of surface roughness versus the fiber orientation angle and depth of cut are plotted in Fig. 14. It is known that the surface roughness increases with fiber orientation from 45° to 135°, as shown in Fig. 14a, and increases slightly with increasing depth of cut in Fig. 14b.

As shown in Fig. 15, the multi-factorial analysis based on the orthogonal design of experiment was applied to investigate the effects of multiple machining parameters and their coupling effects on the surface roughness. The results of multi-factorial ANOVA for surface roughness are given in Table 5. It was noted that fiber orientation angle, cutting

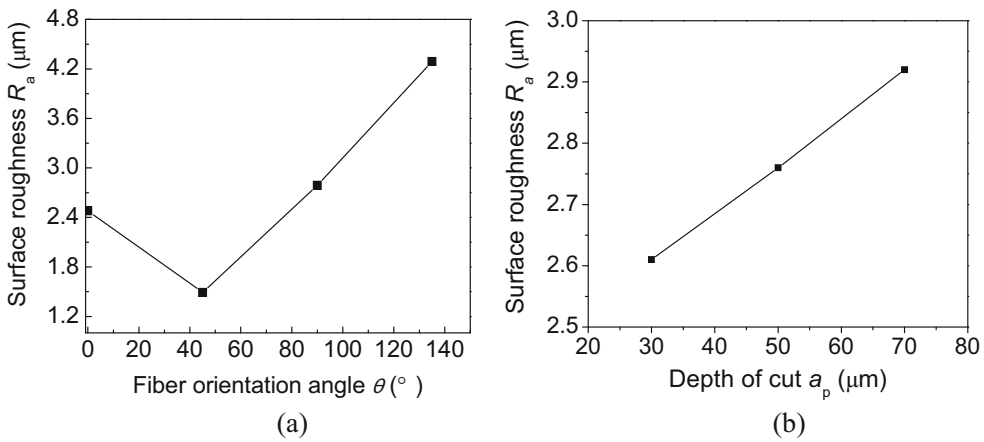

Fig. 14 Dependence of surface roughness on **a** fiber orientation angle and **b** depth of cut

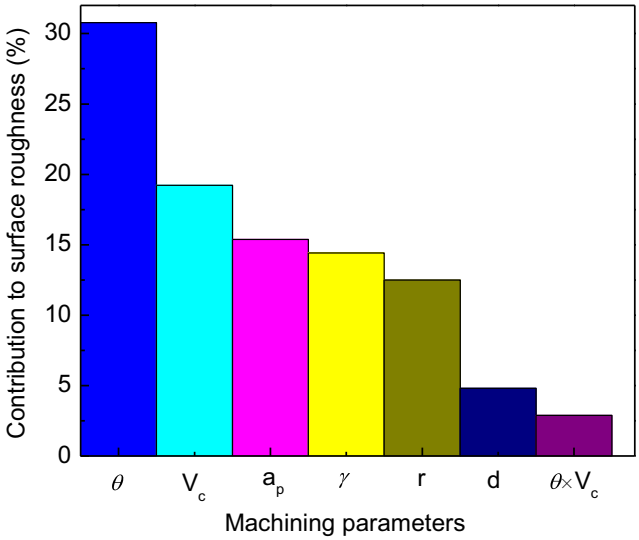

Fig. 15 Quantitative comparison of the contribution of different machining parameters to surface roughness

speed, and depth of cut are the most significant factors affecting the surface roughness and that the coupling effects of the two factors (such as fiber orientation and cutting speed) are also relatively small.

6 Conclusions

This paper studied the effects of multiple machining parameters on the key responses of the unidirectional CFRP composites based on FE simulations by a 3D micromechanical cutting model with consideration of the three constituents of FRP composites as well as temperature. The experimental observations of machined surface were carried out for the validation of FE results. And, then the ANOVA was used to make a quantitative comparison of the influences of multiple machining parameters. The main conclusions have been summarized as follows:

The machined surfaces at different fiber orientations were firstly measured by SEM observation and surface roughness instrument. It was found that there are different surface profiles at different cases, and the machined surface is relatively smooth at 45° while uneven at 135°. Various subsurface damage forms such as interfacial debonding, matrix cracking, and fiber pullout were observed too in our measurement. Furthermore, both of the characteristics of these surfaces and subsurface damage forms predicted in our FE simulations show a very good agreement with the measured results, which successfully demonstrates the reliability of our FE model.

The single-factor analyses of the effects of three key machining parameters (i.e., the cutting speed, the fiber orientation angle, and depth of cut) on the cutting force and surface roughness were then carried out based on the FE simulation results, respectively.

It was indicated that the cutting force increases with increasing cutting speed as well as depth of cut and arrives at the minimum value at 45° while the maximum at 90°. Surface roughness gradually decreases with increasing cutting speed while slightly increases with the depth of cut and is relatively smooth at 45° while uneven at 135°. In addition, different chip morphologies were observed in the chip formation simulation at different fiber orientations, and various failure modes appear correspondingly.

Finally, multi-factorial analyses based on the orthogonal design of experiment and the ANOVA were performed to determine and provide a quantitative comparison of the dominant machining parameters which are affecting the cutting force and surface roughness. The fiber orientation angle in the CFRP composites proves to be the most important factor affecting the cutting force and surface roughness. The next significant factors are the depth of cut and cutting speed for the cutting force while the cutting speed and depth of cut for the surface roughness. The coupling effects of these parameters are actually small and can be neglected in the CFRP machining process.

Table 5 Results of the analysis of variance for surface roughness

Machining parameters	Sum of squares (SS_B)	Degrees of freedom	Mean square (MS_B)	F value	p value
Fiber orientation angle (θ)	12.06	3	4.02	3.325	0.000
Cutting speed (V_c)	5.02	2	2.51	2.251	0.000
Depth of cut (a_p)	4.02	2	2.01	1.713	0.000
Rake angle (γ)	1.88	1	1.88	1.567	0.000
Edge radius (r)	1.63	1	1.63	1.328	0.000
Fiber diameter (d)	0.628	1	0.628	0.492	0.001
Interaction ($\theta \times V_c$)	2.256	6	0.376	0.247	0.002

Acknowledgments This research work was supported by the National Natural Science Foundation of China (No. 11272286 and No. 51375234), the Zhejiang Provincial Natural Science Foundation of China for Distinguished Young Scholars (LR13E050001), and the Open Foundation of State Key Lab of Explosion Science and Technology of China (No. KFJJ14-9M).

References

1. Salonitis K, Pandremenos J, Paralikas J, Chryssolouris G (2010) Multifunctional materials: engineering applications and processing challenges. Int J Adv Manuf Technol 49(5–8):803–826
2. Golzar M, Poorzeinolabedin M (2010) Prototype fabrication of a composite automobile body based on integrated structure. Int J Adv Manuf Technol 49(9–12):1037–1045
3. Haddad M, Zitoune R, Bougherar H, Castanié EF (2014) Study of trimming damages of CFRP structures in function of the machining processes and their impact on the mechanical behavior. Compos Part B 57:136–143
4. Tsao CC (2008) Thrust force and delamination of core-saw drill during drilling of carbon fiber reinforced plastics (CFRP). Int J Adv Manuf Technol 37(1–2):23–28
5. Shahrajabian H, Hadi M, Farahnakian M (2012) Experimental investigation of machining parameters on machinability of carbon fiber/epoxy composites. Int J Eng Innovative Technol 2(3):30–36
6. Farshbaf Zinati R, Razfar MR (2014) Experimental and modeling investigation of surface roughness in end-milling of polyamide 6/multi-walled carbon nano-tube composite. Int J Adv Manuf Technol 75(5–8):979–989
7. Azmi AI, Lin RJT, Bhattacharyya D (2013) Machinability study of glass fibre-reinforced polymer composites during end milling. Int J Adv Manuf Technol 64(1–4):247–261
8. Bagci E, Isik B (2006) Investigation of surface roughness in turning unidirectional GFRP composites by using RS methodology and ANN. Int J Adv Manuf Technol 31(1–2):10–17
9. Abhishek K, Datta S, Mahapatra SS (2013) Response surface modeling on machining of CFRP composites: effect of process variables on surface roughness, MRR and tool-tip temperature. Int J Mech Eng Res 3(4):407–414
10. Palanikumar K (2008) Application of Taguchi and response surface methodologies for surface roughness in machining glass fiber reinforced plastics by PCD tooling. Int J Adv Manuf Technol 36(1–2):19–27
11. Pecat O, Rentsch R, Brinksmeier E (2012) Influence of milling process parameters on the surface integrity of CFRP. Proc CIRP 1:466–470
12. Chakladar ND, Pal SK, Mandal P (2012) Drilling of woven glass fiber-reinforced plastic-an experimental and finite element study. Int J Adv Manuf Technol 58(1–4):267–278
13. Sorrentino L, Turchetta S (2014) Cutting forces in milling of carbon fibre reinforced plastics. Int J Manuf Eng 14:1–8
14. Rao GVG, Mahajan P, Bhatnagar N (2007) Micro-mechanical modeling of machining of FRP composites-cutting force analysis. Compos Sci Technol 67(3–4):579–593
15. Mkaddem A, Demirci I, El Mansori M (2008) A micro–macro combined approach using FEM for modelling of machining of FRP composites: cutting forces analysis. Compos Sci Technol 68(15–16):3123–3127
16. Yang SB, Xu JH, Fu YC, Wei WH (2012) Finite element modeling of machining of hydrogenated Ti-6Al-4V alloy. Int J Adv Manuf Technol 59(1–4):253–261
17. Kalla D, Sheikh-Ahmad J, Twomey J (2010) Prediction of cutting forces in helical end milling fiber reinforced polymers. Int J Mach Tool Manuf 50(10):882–891
18. Jahromi AS, Bahr B (2010) An analytical method for predicting cutting forces in orthogonal machining of unidirectional composites. Compos Sci Technol 70:2290–2297
19. Zhang L (2009) Cutting composites: a discussion on mechanics modeling. J Mater Process Tech 209(1):4548–4552
20. Lasri L, Nouari M, El Mansori M (2009) Modelling of chip separation in machining unidirectional FRP composites by stiffness degradation concept. Compos Sci Technol 69(5):684–692
21. Calzada KA (2012) Modeling and interpretation of fiber orientation-based failure mechanisms in machining of carbon fiber-reinforced polymer composites. J Manuf Process 14(2):141–149
22. Zitoune R, Collombet F, Lachaud F (2005) Experiment-calculation comparison of the cutting conditions representative of the long fiber composite drilling phase. Compos Sci Technol 65(3–4):455–466
23. Santiuste C, Olmedo A, Soldani X, Miguélez H (2012) Delamination prediction in orthogonal machining of carbon long fiber-reinforced polymer composites. J Reinf Plast Compos 31(13):875–885
24. Iliescu D, Gehin D, Iordanoff I, Girot F, Gutierrez M (2010) A discrete element method for the simulation of CFRP cutting. Compos Sci Technol 70(1):73–80
25. Dandekar C, Shin Y (2008) Multiphase finite element modeling of machining unidirectional composites: prediction of debonding and fiber damage. J Manuf Sci Technol 130:1–12
26. Chippendale RD, Golosnoy IO, Lewin PL (2014) Numerical modelling of thermal decomposition processes and associated damage in carbon fibre composites. J Phys D Appl Phys 47:301–315
27. Huang XG, Gillespie JW Jr, Bogetti T (2000) Process induced stress for woven fabric thick section composite structures. Compos Struct 49:303–312
28. Wang Y, Hahn TH (2007) AFM characterization of the interfacial properties of carbon fiber reinforced polymer composites subjected to hygrothermal treatment. Compos Sci Technol 67(26):92–101
29. Zhou P, Zhao FL (2010) The 3D evaluation method of cutting surface topography of carbon/carbon(C/C) composite. High Technol Lett 16(4):366–372
30. Khamel S, Ouelaa N, Bouacha K (2012) Analysis and prediction of tool wear, surface roughness and cutting forces in hard turning with CBN tool. J Mech Sci Technol 26(11):3605–3616